TIME-TO-DEPTH CONVERSION USING MODELING RAYS

T. A. Coimbra, J. H. Faccipieri Junior, and M. Tygel

email: *tgo.coimbra@gmail.com, jorge.faccipieri@gmail.com, tygel@ime.unicamp.br*
keywords: *Time conversion, time migration, image ray, modeling ray*

ABSTRACT

Time-to-depth imaging of time-migrated data is widely used to provide first depth images in a fast and efficient way. As appealing time-to-depth conversion technique is based on so-called modeling rays. One of the techniques to carry out depth and advance time-to-depth conversion by means of so-called modeling rays. This approach avoids the construction of image rays, thus avoiding its disadvantages, which include problems of caustics, interpolation and regularization that are characteristic of image ray-tracing techniques. Besides a review of the concept and tracing of modeling rays, we propose a new algorithm for time-to-depth conversion that is simpler and more efficient than the ones available in the literature. Applications to synthetic and real data provide encouraging results.

INTRODUCTION

In the seventies, Hubral (1977) introduced the image-ray concept, that provided a well-needed geophysical meaning to the time-migration (Kirchhoff) procedure overall used in practice. More specifically it provided the understanding of why the stacking along a diffraction curve (or surface) followed by assigning the result on its apex was the right thing to do. Since that time, the image-ray concept is widely used, not only for time migration, but also for other applications. A good example of that is provided by ray tomography. In the same way as normal rays makes the connection between a zero-offset (ZO) (stacked) volume to a corresponding depth model (see, e.g. Duveneck, 2004), image rays provide an analogous task having time-migrated volumes as input (Dell et al., 2014).

Image rays play also a significant role in (non-tomographic) time-to-depth conversion. That means transforming selected time-migrated reflections or a full time-migrated volume into their corresponding depth-domain counterparts, namely depth images of selected reflectors (see, e.g., Ursin, 1982; Tygel et al., 2011, 2012) or a full depth volume(see, e.g., Cameron et al., 2007, 2008; Iversen and Tygel, 2008).

All the above papers are based on algorithms that, starting from stacked or time-migrated volumes and their respective velocities, are able to trace normal or image rays into depth, as well as simultaneously obtain interval velocity along these rays. In the process, the classic paraxial ray theory (see, e.g., Červený, 2001) for the kinematic and dynamic ray tracing. In this context, it is worth mentioning the important result obtained in Cameron et al. (2007, 2008), by which the (depth) interval velocity along an image ray relates to the time-migration velocity along the time-migrated trace specified by that image ray. That relationship is expressed by a so-called velocity-spreading factor, that varies along the image ray. Although that result is very relevant from the theoretical point view, so far no satisfactory method exists for a reliable estimation of the velocity spreading factor in practice. That partly explains why the methodologies in Cameron et al. (2007, 2008) and Iversen and Tygel (2008) present unpleasant instabilities characteristic of ill-posed problems.

A different approach has been proposed in da Silva et al. (2009). That is based on the introduction of so-called *modeling rays*, which are traced in the time domain. Modeling rays can be understood of duals of image rays, which are traced in depth domain. In the same way that the samples of a single trace in the time-migrated volume gives rise to a single image ray in depth, points along a single vertical in depth gives

rise to a single modeling ray in the time-migrated volume. In the approach used by da Silva et al. (2009), the time-to-depth conversion is carried out by assigning at samples of a vertical line in depth velocity values that relate to time samples along the modeling ray that corresponds to that vertical in depth. Tracing of modeling rays utilizes the so-called wavefront construction theory (Vinje et al., 1993), together with a finite-difference algorithm adapted from Sava and Fomel (2001). The formulation in da Silva et al. (2009) is quite appealing and should have received more attention in the literature. Even though that formulation does not take into account the velocity spreading factor (which amounts as being assumed equal to unity), its practical results are still very valuable.

In this work, we revisit the time-to-depth conversion of da Silva et al. (2009) and advance it in some aspects. From the theoretical side, the modeling-ray equations, originally presented in 2D, have been extended to 3D and generalized so that the velocity-spreading factor, linking the time migration and depth interval velocities, is taken into account. On the practical side, still considering that factor as unity and also in the 2D situation, a simpler and more stable (regularization free) algorithm has been introduced for the modeling ray tracing. The reliable estimation of that factor, is a topic of ongoing research. In spite of that limitation, applications to synthetic and real data provide encouraging results.

FORMULATION

We formulate the time-to-depth conversion of a time-migrated volume under the use of modeling rays. Our reference is da Silva et al. (2009). We start with the introduction of appropriate coordinate systems and proceed with the definition of image and modeling rays. Based on such considerations, the description of the time-to-depth conversion algorithm will be provided in the next section.

Coordinate systems: We consider two Cartesian coordinate systems, one for the depth domain and another for the time-migrated domain. More specifically, we have:

(a) Points in the depth domain are given by coordinates (x, y, z), where x e y are lateral coordinates and z is depth. In that domain, the image rays are to be traced;

(b) Points in the time-migrated domain are given by coordinates (ξ, η, τ), where ξ (inline) and η (crossline) specify the time-migrated trace and τ the (two-way) migrated time. In that domain, the modeling rays are to be traced.

Image rays: In this work, we suppose that wave propagation is conveniently modeled by the acoustic wave equation. Assuming for simplicity a constant density and a variable velocity, $v = v(x, y, z)$, the equation for pressure, $P(x, y, z, \tau)$, is given by

$$\frac{\partial^2 P}{\partial x^2} + \frac{\partial^2 P}{\partial y^2} + \frac{\partial^2 P}{\partial z^2} - \frac{1}{v^2}\frac{\partial^2 P}{\partial \tau^2} = 0\,, \tag{1}$$

together with boundary and initial conditions. As well known (see, e.g., Červený, 2001), convenient, so-called *ray solutions* of Equation wave can be obtained under in the form

$$P(x, y, z, \tau) = Re\{A(x, y, z)F(\tau - \mathcal{T}(x, y, z))\}\,, \tag{2}$$

where $A(x, y, z)$ represents an amplitude (complex) factor, $\mathcal{T}(x, y, z)$ is an (real) traveltime (of phase) and $F(\tau)$ is an analytic (complex) pulse shape, the latter being directly obtained from the (real) observed source pulse. In the modeling, the function $F(\tau)$, is assumed to be known. For our purposes, we are only interested in the traveltime function, $\mathcal{T}(x, y, z)$, from which the ray trajectories are determined. Observe that, for constant τ, the equation

$$\mathcal{T}(x, y, z) = \tau\,, \tag{3}$$

represents the wavefront of the ray solution (3) at the time τ. The equations for the phase, $\mathcal{T}(x, y, z)$, and amplitude, $A(x, y, z)$, are obtained through the substitution of the ray expression (3) into the wave

equation (1). As well known (see, e.g., Červený, 2001), the traveltime, $calT(x, y, z)$, satisfies the so-called *eikonal equation*

$$\mathcal{T}_x^2 + \mathcal{T}_y^2 + \mathcal{T}_z^2 = \frac{1}{v^2}\,, \tag{4}$$

where $\mathcal{T}_x = \partial\mathcal{T}/\partial x$, $\mathcal{T}_y = \partial\mathcal{T}/\partial y$ e $\mathcal{T}_z = \partial\mathcal{T}/\partial z$, together with boundary and initial conditions. Still following Červený (2001), the eikonal equation can be solved by means of the introduction of *rays*. These are temporal curves $\mathbf{x}(\tau) = (x(\tau), y(\tau), z(\tau))$, that satisfy the *ray-tracing system* given by

$$\begin{aligned} &\frac{dx}{d\tau} = v^2\mathcal{T}_x, \quad \frac{dy}{d\tau} = v^2\mathcal{T}_y, \quad \frac{dz}{d\tau} = v^2\mathcal{T}_z\,, \\ &\frac{d\mathcal{T}_x}{d\tau} = -\frac{1}{v^2}v_x, \quad \frac{d\mathcal{T}_y}{d\tau} = -\frac{1}{v^2}v_y, \quad \frac{d\mathcal{T}_z}{d\tau} = -\frac{1}{v^2}v_z\,, \end{aligned} \tag{5}$$

where $v_x = \partial v/\partial x$, $v_y = \partial v/\partial y$ and $v_z = \partial v/\partial z$, all quantities being evaluated at $(x(\tau), y(\tau), z(\tau))$.

For the *image ray*, we have an advantageous characteristic: The slowness vector is normal at its initial pint at the measurement surface, is normal to that surface. Assuming, for simplicity, that the measurement surface is a horizontal plane, $z = 0$, that the ray initial point has coodinates $x = \xi$, $y = \eta$ e $z = 0$, and that the velocity at that initial point is v_0, we obtain the initial conditions

$$\begin{aligned} &x(0) = x_0, \quad y(0) = y_0, \quad z(0) = 0\,, \\ &\tau_x(0) = 0, \quad \tau_y(0) = 0, \quad \tau_z(0) = 1/v_0\,. \end{aligned} \tag{6}$$

Modeling rays: Introduced by da Silva et al. (2009), the *modeling rays*, which propagate in the time-migrated domain, have a strong analogy (referred here as *duality*) with the image rays, which propagate in depth domain. As opposed to, e.g., Cameron et al. (2007), Iversen and Tygel (2008) and Gelius and Tygel (2015), that propose time-to-depth conversion of time-migrated volumes algorithms based on image rays, we follow the counterpart approach of da Silva et al. (2009) that is based on modeling rays.

As shown in Appendix A, modeling rays are determined by a so-called *modeling eikonal equation*. In Appendix B, we derive the (most simple) *modeling wave equation* for which ray theory yields that eikonal.

In this work, initial, proof-of-concept, implementations and tests of the proposed time-to-depth algorithm are considered under In this situation, our modeling wave equation is given by (see Appendix B)

$$\frac{\partial^2\bar{P}}{\partial\xi^2} + \frac{\partial^2\bar{P}}{\partial\eta^2} + \frac{1}{v_{Dix}^2}\frac{\partial^2\bar{P}}{\partial\tau^2} - \frac{\partial^2\bar{P}}{\partial z^2} = 0\,. \tag{7}$$

Here, $\bar{P} = \bar{P}(\xi, \eta, \tau, z) = P(x(\xi, \eta), y(\xi, \eta), z, \tau)$ represents pressure and $v_{Dix}(\xi, \eta, \tau)$ the time interval velocity (*Dix velocity*), both computed in time-migrated domain coordinates. More specifically,

$$v_{Dix}^2(\xi, \eta, \tau) = \det \mathbf{V}_{Dix}\,, \tag{8}$$

where $\mathbf{V}_{Dix}$ is the interval time velocity, 2×2 symmetric matrix, obtained by the Dix transformation (see, e.g., Cameron et al., 2007; Gelius and Tygel, 2015),

$$\det\left(\mathbf{V}_{Dix}^2\right) = \det\left(\frac{\partial}{\partial\tau}[\tau\mathbf{V}_M^2(\xi, \eta, \tau)]\right)\,, \tag{9}$$

applied to the time-migration velocity matrix, $\mathbf{V}_M$. Observe that the modeling wave, which propagates in the time domain, has as propagation variable the depth coordinate, z. As a counterpart, the image wave, which propagates in the depth domain, has as propagation variable, the temporal coordinate, τ. In agreement with the above observation, the eikonal that govern modeling rays is determined by substituting into the modeling wave equation (7), the ray solution (compare with Equation (2))

$$\bar{P}(\xi, \eta, \tau, z) = Re\{B(\xi, \eta, \tau)F(z - Z(\xi, \eta, \tau))\}\,. \tag{10}$$

Here, $B(\xi,\eta,\tau)$ represents an amplitude, $Z(\xi,\eta,\tau)$ a *depth phase* and $F(z)$ is an analytic depth pulse. Observe that, for each depth value, z, the equation

$$Z(\xi,\eta,\tau) = z\,, \tag{11}$$

represents a wavefront at the *depth instant*, z. Still under the assumption of a locally laterally homogeneous media, the depth phase, $Z(\xi,\eta,\tau)$, must satisfy the modeling eikonal (compare with the image-ray eikonal of Equation (4))

$$Z_\xi^2 + Z_\eta^2 + \frac{1}{v_{Dix}^2} Z_\tau^2 = 1\,. \tag{12}$$

where $Z_\xi = \partial Z/\partial\xi$, $Z_\eta = \partial Z/\partial\eta$ e $Z_\tau = \partial Z/\partial\tau$. The above eikonal permits one to determine the modeling ray, $\boldsymbol{\xi}(z) = (\xi(z),\eta(z),\tau(z))$, by means of the ray-tracing system

$$\begin{aligned} &\frac{d\xi}{dz} = Z_\xi, \quad \frac{d\eta}{dz} = Z_\eta, \quad \frac{d\tau}{dz} = \frac{1}{v^2} Z_\tau\,, \\ &\frac{dZ_\xi}{dz} = \frac{Z_\tau^2}{v^3} v_\xi, \quad \frac{dZ_\eta}{dz} = \frac{Z_\tau^2}{v^3} v_\eta, \quad \frac{dZ_\tau}{dz} = \frac{Z_\tau^2}{v^3} v_\tau\,. \end{aligned} \tag{13}$$

together with the initial conditions

$$\begin{aligned} &\xi(0) = \xi_0, \quad \eta(0) = \eta_0, \quad \tau(0) = 0\,, \\ &Z_\xi(0) = 0, \quad Z_\eta(0) = 0, \quad Z_\tau(0) = v_0\,. \end{aligned} \tag{14}$$

Slowness vectors: An important role in ray theory is played by *slowness vectors*. At each point of propagation, the slowness vector points normal to the ray wavefront. Introducing the notations $\mathbf{p}^{(x)} = \mathbf{p}^{(x)}(x,y,z)$ e $\mathbf{p}^{(\xi)} = \mathbf{p}^{(\xi)}(\xi,\eta,\tau)$ for the slowness vectors of the image and modeling rays, respectively, we find the relations

$$\begin{aligned} \mathbf{p}^{(x)} &= \nabla_x \tau = (\tau_x, \tau_y, \tau_z)\,, \\ \mathbf{p}^{(\xi)} &= \nabla_\xi Z = (Z_\xi, Z_\eta, Z_\tau)\,. \end{aligned} \tag{15}$$

Observe that the slowness vector of the image ray, $\mathbf{p}^{(\mathbf{x})}$, has, as expected, the dimensions of inverse velocity. However, the slowness vector of the modeling ray, $\mathbf{p}^{(\xi)}$, has the first two coordinates, Z_ξ e Z_η, non dimensional and the third one, Z_τ, with dimension of velocity inverse. Is spite of this "dimensionality abuse", we found it convenient to maintain the terminology os slowness also for that case. In view of the above definitions, we can express the initial conditions for the ray tracing of image rays (Equation (6)) and modeling rays (Equation 14), in the form

$$\begin{aligned} &\mathbf{x}(0) = (x_0, y_0, 0), \quad \mathbf{p}^{(x)}(0) = (0, 0, 1/v_0)\,, \\ &\boldsymbol{\xi}(0) = (\xi_0, \eta_0, 0), \quad \mathbf{p}^{(\xi)}(0) = (0, 0, v_0)\,. \end{aligned} \tag{16}$$

We assum that for both image and modeling rays, the slownness vectors are normal to the measurement surface $z = \tau = 0$.

CONVERSION ALGORITHM

In view of the above formulation, we are now ready to describe the proposed time-to-depth conversion algorithm. We consider the time-migrated volume, which consists of amplitudes $u(\xi,\eta,\tau)$ and time-migration velocities, $v_M(\xi,\eta,\tau)$, where (ξ,η) denotes the trace and τ the (two-way) migration time. We also consider that the migration velocity has been already transformed to interval time (Dix) velocity, $v_{Dix}(\xi,\eta,\tau)$, as computed by Equation (8). We finally suppose that the coordinates (x,y,z) specify the depth-domain points where the conversion will take place.

For a grid depth points (x_i, y_j, z_k), the envisaged algorithm consis in assigning an amplitude, $u(x_i, y_j, z_k)$, and a velocity, $v(x_i, y_j, z_k)$ to each grid point. We consider that the amplitude and interval time (Dix) velocity (obtained from the time-migration velocity field) are given on a user-selected grid of points, $u(\xi_p, \eta_q, \tau_r)$.

The assignment of amplitudes and velocities in the depth domain will be carried out along each trace, (x_i, y_j), at the acquisition plane, $z = 0$, at samples, z_k, along the depth vertical coordinate, z, by means of the following procedure:

(1) Trace modeling ray, $(\xi(z), \eta(z), \tau(z))$, in the time-migrated domain, starting from the point, $\xi(0) = x_i$, $\eta(0) = y_i$ and $\tau(0) = 0$;

(2) At the point, $(\xi(z_k), \eta(z_k), \tau(z_k))$, on the modeling ray, compute the amplitude and time interval (Dix) velocity, obtained by interpolating the corresponding values at neighboring points at the given grid in the time-migrated domain.

(3) The obtained values of amplitude and velocity will be assigned at the depth point $(\xi(z_k), \eta(z_k), \tau(z_k))$.

RESULTS

Our time-to-depth conversion was implemented using the software Matlab® and tested in a preliminary way in 2D synthetic and real data. The main objective of the synthetic experiments was to validate the developed theory, by comparing the time-to-depth results with the original geological models. After validation, the algorithm was tested for a real dataset followed by a discussed of the obtained results. In all following figures, the time axis represent *one-way time*. Velocities are given in km/s.

Synthetic examples: For the synthetic examples below, we make the following considerations:

(a) For any depth point, $D = (x, y, z)$, we assume that the depth velocity equals the interval time (Dix) velocity at the corresponding point, (ξ, η, τ), in the time-migrated domain that is determined by the image ray traced from D to the acquisition surface. More specifically, (ξ, η) represents the point where the image ray from D hits the acquisition surface, with τ being the (two-way) traveltime along that ray.

(b) Once the Dix velocity field is obtained, the proposed time-to-depth algorithm is used to map these velocities along the modeling rays for all points of the time-migrated domain.

Remark: The construction indicated above may seem artificial since it differs from the real situation. In practice, the time-migration velocity field is the given input data, which is transformed into is corresponding interval time (Dix) velocity field. The obtained interval time velocity field represents the *input* for the proposed conversion algorithm. Even with this limitation, the synthetic examples work well as “proof of concept" for our scheme. In the real-data example, the correct application of the algorithm is undertaken.

(1) **First synthetic example:** The depth-velocity field is laterally invariant, being given by

$$v(z) = 1500 + 0.5z\,, \tag{17}$$

as shown in Figure 1 (Top-Left) in km/s. The corresponding interval time (Dix) velocity field is represented in Figure 1 (Top-Right). The result of the time-to-depth conversion can be seen in Figure 1 (Bottom-Left). The comparison between the original model and the depth-converted is shown in Figure 1 (Bottom-Right). Note that, in this case, the relative error was of the order of 0.1%, which can be considered as a numerical error.

(2) **Second synthetic example:** Our model now has a velocity with lateral and depth variations, being defined by

$$v(x, z) = 1500 + 0.5z + 0.3x\,, \tag{18}$$

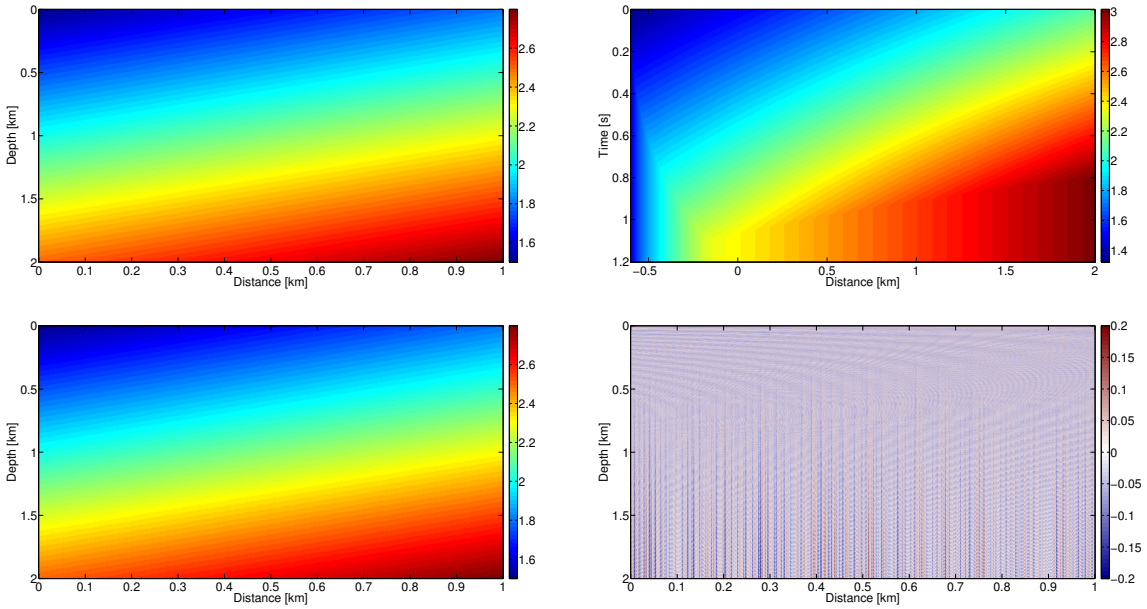

Figure 1: *First synthetic model: (Top-Left) Geological model with laterally and depth varying velocity according to Equation (17) in km/s. (Top-Right) Time velocity field mapped along image rays for the model. (Bottom-Left) Depth velocity field, re-mapped along modeling rays. (Bottom-Right) Percentage relative error, between the results presented in Figure (Top-Left) and Figure (Bottom-Left).*

represented in Figure 2 (Top-Left) in km/s. The corresponding interval time (Dix) velocity field is represented in Figure 2 (Top-Right). The resulting time-to-depth conversion can be seen in Figure 2 (Bottom-Left). Comparison with the original model is shown in Figure 2 (Bottom-Right). Once again, the relative error was very small, of the order of 0.2%, which can be considered as a numerical error.

(3) **Third synthetic example:** Our last synthetic example is more complex, with lateral and depth velocity variation according to the expression

$$v(x,z) = 1000\left\{2 - \exp[(-1.5/1000^2)(x^2 + (z-2000)^2)]\right\}\ , \tag{19}$$

represented in Figure 3 (Top-Left) in km/s. The same previously described procedures have bee applied giving rise to the Figures 3 (Top-Right) and 3 (Bottom-Left). Note that, in this example, the relative error shown in the lower part of Figure 3 (Bottom-Right) is of the order of 3%, hence larger than the previous cases. Away from these regions, the error can still be considered as a numerical error.

To illustrate the above observations, Figures 4 (Top-Left) and (Top-Right) show the image and modeling wavefronts overlaid to the respective velocity fields in depth and interval time. Note that in the regions where the wavefronts have significant curvature, the corresponding image rays widens of compress, as especially seen in the lower-most part of Figure 4 (Bottom-Left). This behavior may affect the velocity information stored at the chosen grid for construction of Figure 3 (Top-Right). The same phenomenon can be observed for the modeling wavefronts, with the difference that, where the image rays compress, the modeling rays widens Figures 4 (Bottom-Left) and (Bottom-Right). As shown in Figures 4 (Bottom-Left and Bottom-Right) there is a concentration of image rays and widening of modeling rays in the lower-most part of these figures. This explains the large 3% error shown in Figure 3 (Bottom- Right).

(4) **Real data example:** Our time-to-depth algorithm is now applied to a real marine data set of the Jequitinhonha basin, Brazil. The time-migrated image, as well as the time-migration velocity field

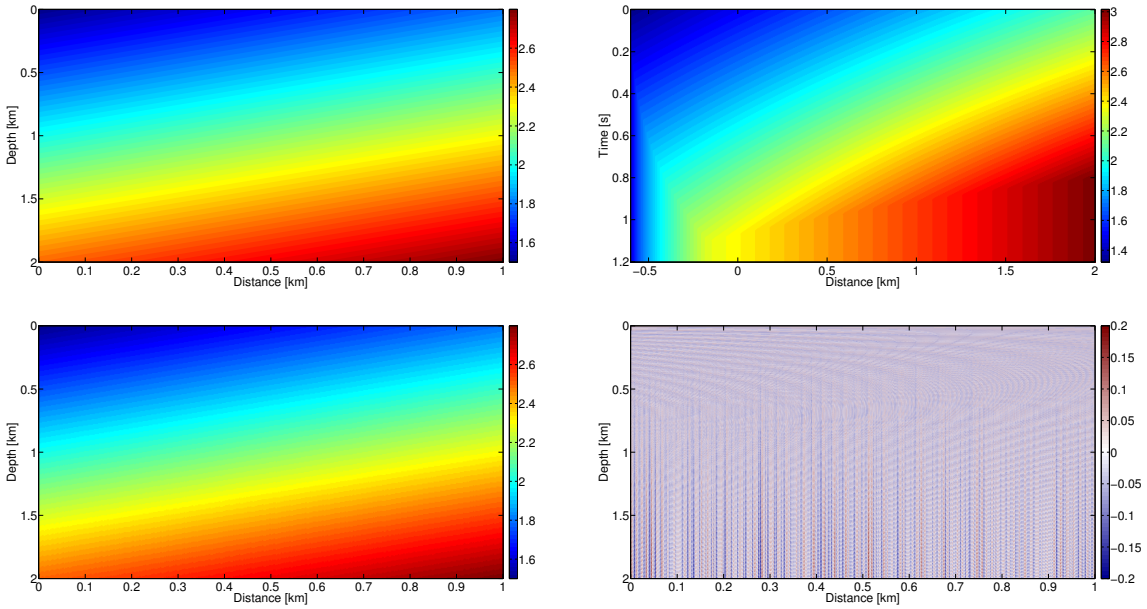

Figure 2: *Second synthetic model: (Top-Left) Geological model with laterally and depth varying velocity according to Equation (18) in km/s. (Top-Right) Time velocity field mapped along image rays for the model. (Bottom-Left) Depth velocity field, re-mapped along modeling rays. (Bottom-Right) Percentage relative error, between the results presented in Figure (Top-Left) and Figure (Bottom-Left).*

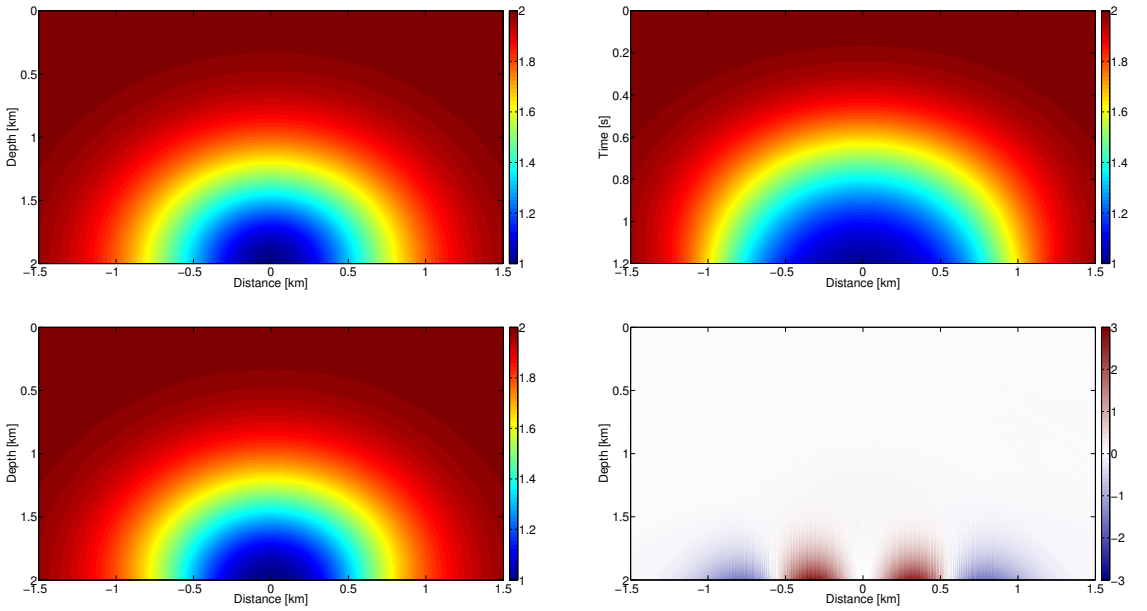

Figure 3: *Third synthetic model: (Top-Left) Geological model with laterally and depth varying velocity according to Equation (19) in km/s. (Top-Right) Time velocity field mapped along image rays for the model. (Bottom-Left) Depth velocity field, re-mapped along modeling rays. (Bottom-Right) Percentage relative error, between the results presented in Figure (Top-Left) and Figure (Bottom-Left).*

can be seen in Figures 5 and 6, respectively.

The time-migration velocities were transformed to their corresponding interval (Dix) time-velocities

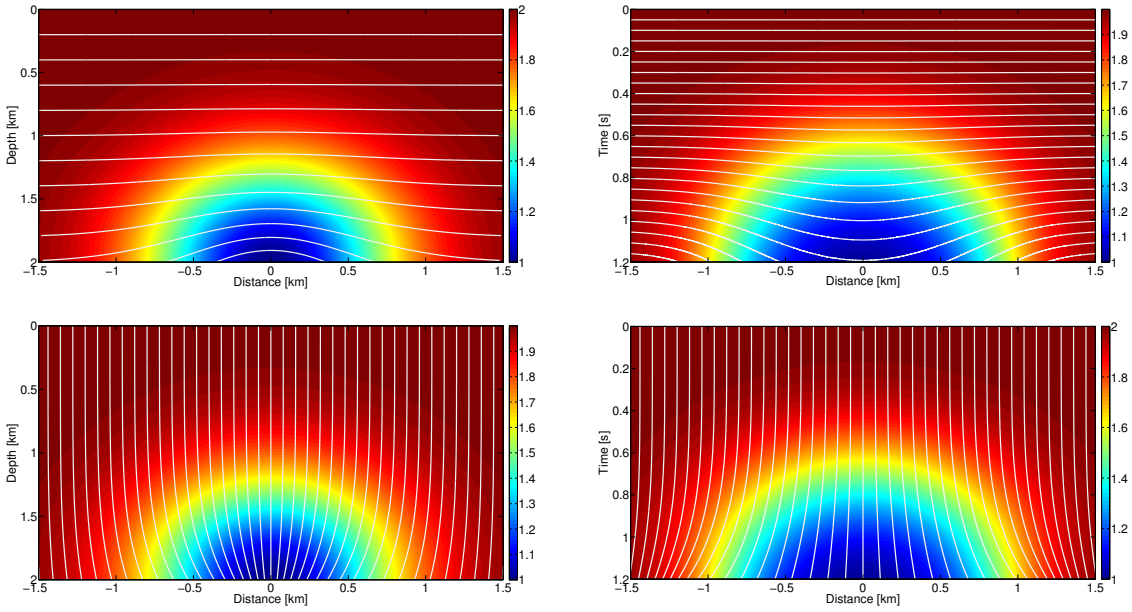

Figure 4: *Third synthetic model: (Top-Left) Image wavefronts in time intervals of* 0.1 *s (blue lines), overlaid to depth-velocity model. (Right-Top) Modeling wavefronts in depth intervals of* 100 *m (blue lines), overlaid to interval (Dix) time-velocity model. (Left-Bottom) Tracing image rays in depth. (Right-Bottom) Tracing modeling rays in time.*

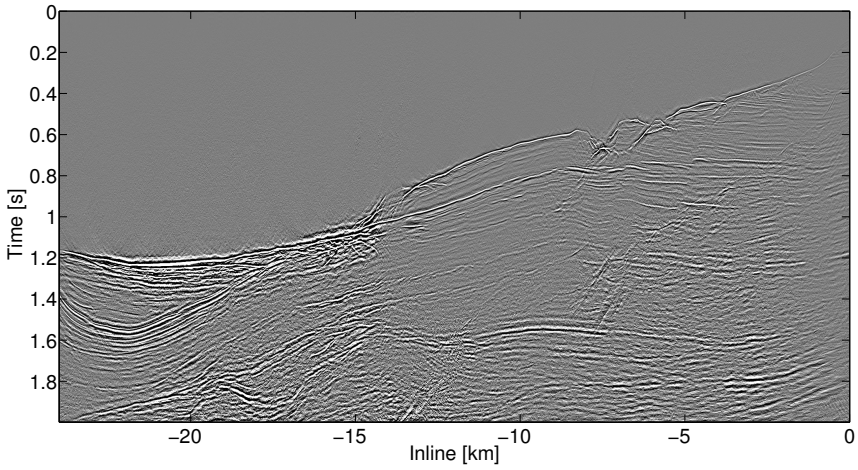

Figure 5: *Real data: Prestack time migration of a marine seismic line of the Jequitinhonha basin, Brazil.*

shown in Figure 7). These velocities were, in turn, converted into depth along modeling rays. The result is shown in Figure 8.

Depth conversion was finally applied to the time-migrated data of Figure 5, the result shown in Figure 9. For comparison, Figure 10 shows the conventional (Kirchhoff) poststack depth migration of the original data. We can observe that, except for the previously cited regions, the events are well positioned laterally and in depth.

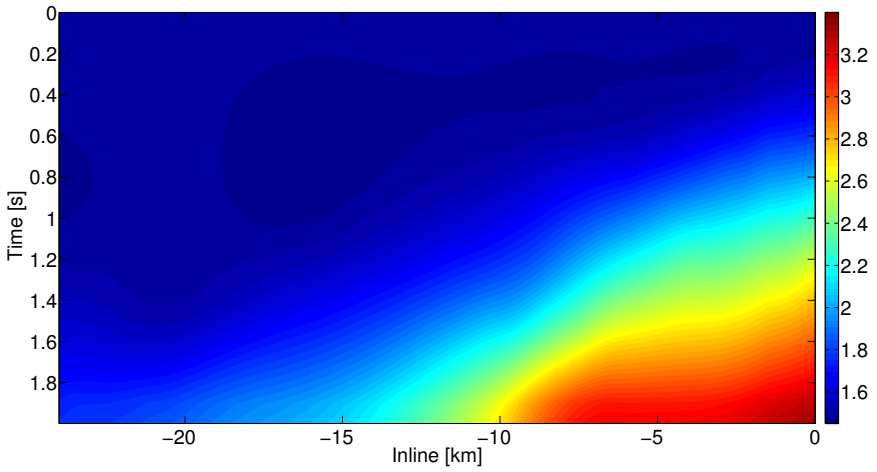

Figure 6: *Real data: Time-migration velocity field.*

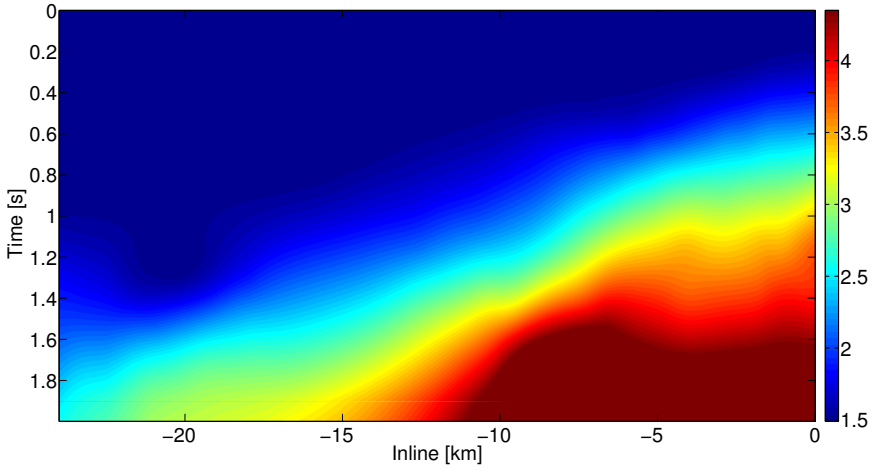

Figure 7: *Real data: Interval (Dix) time-velocity field derived from the time-migration velocity field of Figure 6.*

DISCUSSION

The above presented time-to-depth algorithm transfers to depth the interval (Dix) time velocity obtained from the time-migration process. This means that we suppose that we suppose that the depth velocity at each point of an image ray coincides with the interval time velocity that refers to the corresponding point in the time-migrated domain. As shown in Cameron et al. (2007, 2008), and based on the paraxial ray theory, these two velocities do not coincide, being related by a correction factor (referred to as velocity spreading factor), which depends on attributes the dynamic ray tracing of the image rays. In view of the good results obtained in da Silva et al. (2009), in which that correction factor is neglected (i.e., taken as unity), and moreover that, under that in this case the conversion algorithm is far simpler, we adopted in our implementation the above described coincidence of depth and interval time velocities. Nevertheless, we maintain our investigations with the aim of accounting the velocity spreading factor in the conversion algorithm, as well as estimating its influence in the conversion results.

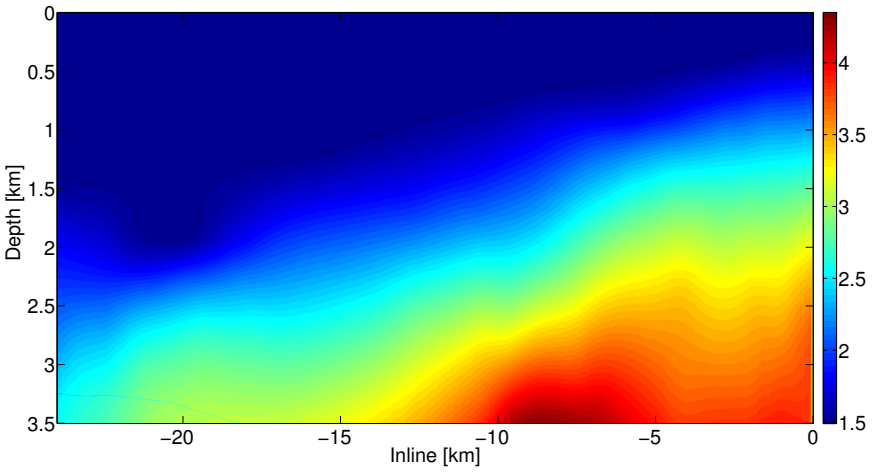

Figure 8: *Real data: Depth-velocity field re-mapped by modeling rays Time-migration velocity field.*

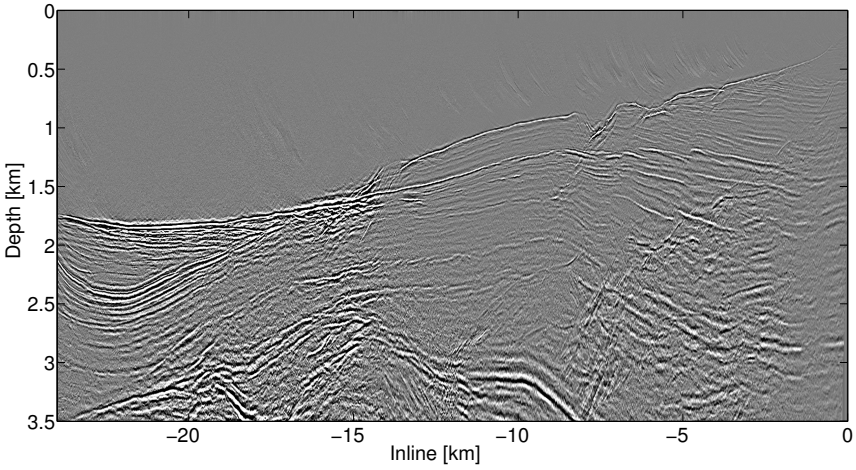

Figure 9: *Real data: Time-to-depth conversion (re-mapping by modeling rays) of time-migrated image shown in Figure 5*

CONCLUSIONS

In this work, we have revisited and improved the methodology of depth conversion of time-migrated volumes by means of modeling rays. Such methodology does not require the construction of image rays, thus avoiding disadvantages characteristic of the techniques that utilize those rays. In an analogous way as in the classical ray theory, modeling rays are associated with (fictitious) modeling wave equations that propagate in time-migrated domain. The propagation velocity of the modeling waves are related to the interval (Dix) time-velocity, which are extracted from time-migration velocities, supposed available from the time-migration process. Besides that, the only requirement is that the time-migration velocities smooth enough to allow for ray-tracing. In fact, the proposed approach requires less velocity smoothness (continuity up to first-derivatives) than the ones the employ image rays (continuity up to second-order derivatives). At the present stage, the our time-to-depth conversion algorithm assumes the condition of locally lateral homogeneity, for which the velocity at each (depth) point of an image ray coincides with the interval

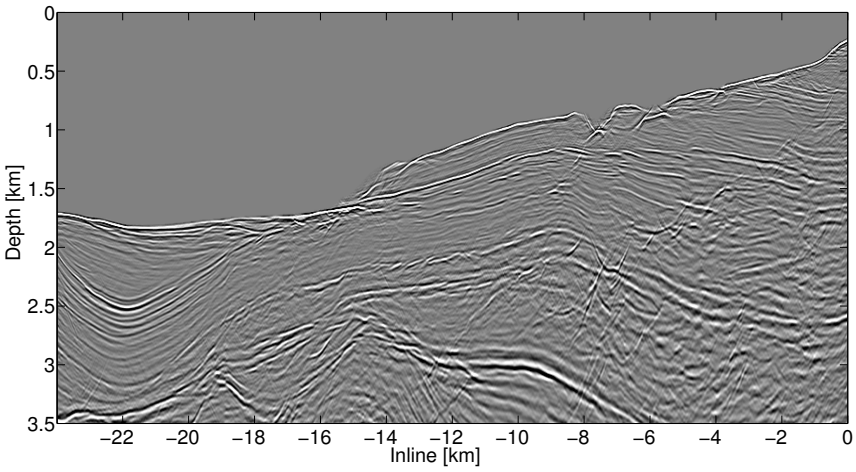

Figure 10: *Real data: Conventional (Kirchhoff) poststack depth migration of original data.*

time-velocity evaluated its corresponding point in the time-migrated domain. We recall that the interval time-velocity is obtained from the time-migrated velocity by means of the so-called Dix transformation.

The contributions of the present paper are twofold. At first, a theoretical review of the 3D propagation of modeling waves and corresponding modeling rays is provided. Secondly, still in the framework of 2D propagation and locally lateral homogeneity, we present a new algorithm, which has better properties of simplicity and efficiency than the one available in the literature. Application to synthetic and real data sets have provided encouraging results.

APPENDIX A: DERIVATION OF MODELING EIKONAL EQUATION

In this appendix, we derive the modeling eikonal equation, namely the one that determines the modeling rays. Our point of departure is Equation (11), recast in the form

$$Z(\xi_1(x_1,x_2,z),\xi_2(x_1,x_2,z),\tau(x_1,x_2,z)) = z\,, \tag{20}$$

where z is a constant. That equation represents the wavefront of a modeling ray at the "instant" z. Applying to both members the partial derivatives with respect to x_1, x_2 e z and with the help of the chain rule of advanced calculus, we find the system

$$\begin{aligned}
\frac{\partial Z}{\partial \xi_1}\frac{\partial \xi_1}{\partial x_1} + \frac{\partial Z}{\partial \xi_2}\frac{\partial \xi_2}{\partial x_1} + \frac{\partial Z}{\partial \tau}\frac{\partial \tau}{\partial x_1} &= 0\,,\\
\frac{\partial Z}{\partial \xi_1}\frac{\partial \xi_1}{\partial x_2} + \frac{\partial Z}{\partial \xi_2}\frac{\partial \xi_2}{\partial x_2} + \frac{\partial Z}{\partial \tau}\frac{\partial \tau}{\partial x_2} &= 0\,,\\
\frac{\partial Z}{\partial \xi_1}\frac{\partial z}{\partial z} + \frac{\partial Z}{\partial z}(\frac{\partial \xi_2}{\partial z} + \frac{\partial Z}{\partial \tau}\frac{\partial \tau}{\partial z} &= 1\,.
\end{aligned} \tag{21}$$

Introducing the gradients

$$\hat{\nabla}_x\xi_i = \left(\frac{\partial \xi_i}{\partial x_1},\frac{\partial \xi_i}{\partial x_2},\frac{\partial \xi_i}{\partial z}\right)^T,\quad \hat{\nabla}_x\tau = \left(\frac{\partial \tau}{\partial x_1},\frac{\partial \tau}{\partial x_2},\frac{\partial \tau}{\partial z}\right)^T,\quad \hat{\nabla}_\xi Z = \left(\frac{\partial Z}{\partial \xi_1},\frac{\partial Z}{\partial \xi_2},\frac{\partial Z}{\partial \tau}\right)^T, \tag{22}$$

the system (21) can be recast in matrix form as

$$\begin{bmatrix}\hat{\nabla}_x\xi_1 & \hat{\nabla}_x\xi_2 & \hat{\nabla}_x\tau\end{bmatrix}\hat{\nabla}_\xi Z = \begin{bmatrix}0 & 0 & 1\end{bmatrix}^T, \tag{23}$$

Left multiplication of equation (23) by its conjugate equation, we readily obtain

$$(\hat{\nabla}_\xi Z)^T \hat{\mathbf{\Lambda}} \, (\hat{\nabla}_\xi Z) = 1 \,, \tag{24}$$

where

$$\begin{aligned} \hat{\mathbf{\Lambda}} &= \begin{bmatrix} \hat{\nabla}_x \xi_1 & \hat{\nabla}_x \xi_2 & \hat{\nabla}_x \tau \end{bmatrix}^T \begin{bmatrix} \hat{\nabla}_x \xi_1 & \hat{\nabla}_x \xi_2 & \hat{\nabla}_x \tau \end{bmatrix} \\ &= \begin{bmatrix} \hat{\nabla}_x \xi_1 \cdot \hat{\nabla}_x \xi_1 & \hat{\nabla}_x \xi_1 \cdot \hat{\nabla}_x \xi_2 & \hat{\nabla}_x \xi_1 \cdot \hat{\nabla}_x \tau \\ \hat{\nabla}_x \xi_2 \cdot \hat{\nabla}_x \xi_1 & \hat{\nabla}_x \xi_2 \cdot \hat{\nabla}_x \xi_2 & \hat{\nabla}_x \xi_2 \cdot \hat{\nabla}_x \tau \\ \hat{\nabla}_x \tau \cdot \hat{\nabla}_x \xi_1 & \hat{\nabla}_x \tau \cdot \hat{\nabla}_x \xi_2 & \hat{\nabla}_x \tau \cdot \hat{\nabla}_x \tau \end{bmatrix} . \end{aligned} \tag{25}$$

The above equation constitutes the modeling eikonal. Our problem reduces, thus, to the determination of the matrix $\hat{\mathbf{\Lambda}}$.

Displacement vector in ray-centered and global coordinates: As shown below, the coefficients of the matrix $\hat{\mathbf{\Lambda}}$ can be determined in a convenient way upon the introduction of the so-called ray-centered local coordinates, (q_1, q_2, q_3), that correspond to a fixed depth point, $D = (x_1, x_2, z)$, on a fixed, central ray, chosen here to be an image ray. As explained in Červený (2001) (see, Section 4.1.4), the ray-centered coordinate system is a moving (positive) Cartesian system along the central ray, such that, at each point D of that ray, we have (a) the q_3-axis points in the direction of the slowness vector of the central ray at D and (b) the (mutually perpendicular) q_1- and q_2-axes belong to the plane normal to the q_3-axis. The position of the q_1- and q_2-axes on the normal plane to the q_3-axis (in principle defined only up to a rotation with respect to that axis) is determined by the initial point of the central ray. More information on the ray-centered coordinate system can be found in Červený (2001).

For a same differential displacement vector, its expressions in global coordinates, $d\hat{\mathbf{x}} = (dx_1, dx_2, dz)^T$ and ray-centered coordinates, $d\hat{\mathbf{q}} = (dq_1, dq_2, dq_3)^T$ satisfy a relation of the form

$$d\hat{\mathbf{q}} = \hat{\mathbf{H}} \, d\hat{\mathbf{x}} \,, \tag{26}$$

in which

$$\hat{\mathbf{H}} = (H_{ij}) = \left(\frac{\partial x_j}{\partial q_i} \right) , \quad i, j = 1, 2, 3. \tag{27}$$

A good insight of the meaning of the matrix $\hat{\mathbf{H}}$ can be grasped by considering the auxiliary matrix $\hat{\mathbf{U}} = (U_{ij})$, $i, j = 1, 2, 3$, defined by

$$\hat{\mathbf{U}} = \hat{\mathbf{H}} \hat{\mathbf{H}}^T = \hat{\mathbf{H}}^T \hat{\mathbf{H}} \,. \tag{28}$$

By the definition (27), we find, using Einstein's rule of multiplication

$$U_{ij} = \left(\frac{\partial x_i}{\partial q_k} \right) \left(\frac{\partial x_j}{\partial q_k} \right) = (\nabla_q x_i) \cdot (\nabla_q x_j) \,. \tag{29}$$

By the fact that the global and ray-centered coordinate systems are positive Cartesian, the above expression yields

$$\hat{\mathbf{U}} = \hat{\mathbf{H}} \hat{\mathbf{H}}^T = \hat{\mathbf{H}}^T \hat{\mathbf{H}} = \hat{\mathbf{I}} \,, \tag{30}$$

where $\hat{\mathbf{I}}$ is the 3×3 identity matrix. With the help of the above, we observe that, for any differentiable function, $f = f(q_1(x_1, x_2, z), q_2(x_1, x_2, z), q_3(x_1, x_2, z))$, we have the important relation

$$\hat{\nabla}_x f = \hat{\mathbf{H}} \, \hat{\nabla}_q f \,, \tag{31}$$

where

$$\hat{\nabla}_x f = (f_{x_1}, f_{x_2}, f_z)^T \quad \text{and} \quad \hat{\nabla}_q f = (f_{q_1}, f_{q_2}, f_{q_3})^T \,, \tag{32}$$

are the gradients of f with respect to coordinates $\hat{\mathbf{x}}$ and $\hat{\mathbf{q}}$, respectively. From Equations (31) and (32), it follows that, for any other differentiable function, $g = g(q_1(x_1, x_2, z), q_2(x_1, x_2, z), q_3(x_1, x_2, z))$, we

readily find

$$\begin{aligned}(\hat{\nabla}_x f)\cdot(\hat{\nabla}_x g) &= (\hat{\nabla}_x f)^T(\hat{\nabla}_x g) = [\hat{\mathbf{H}}\,(\hat{\nabla}_q f)]^T[\hat{\mathbf{H}}\,(\hat{\nabla}_q y)] \\ &= (\hat{\nabla}_q f)^T[\hat{\mathbf{H}}^T\,\hat{\mathbf{H}}](\hat{\nabla}_q g)] = (\hat{\nabla}_q f)^T(\hat{\nabla}_q g) \\ &= (\hat{\nabla}_q f)\cdot(\hat{\nabla}_q g)\,. \end{aligned} \tag{33}$$

As an important consequence of the above equation, is that it enables one to compute the scalar-product components of the sought-for matrix $\hat{\mathbf{\Lambda}}$ of Equation (25) in local ray-centered instead of global coordinates. We show next how that is done.

Displacement vector in ray-centered and time-migration coordinates: We now proceed to find analogous relationships for a same displacement vector in ray-centered coordinates, $\hat{\mathbf{q}} = (q_1, q_2, q_3)^T$ and $\hat{\boldsymbol{\xi}} = (\xi, \eta, \tau)$. In analogy with Equation (26), we write

$$d\hat{q} = \hat{\mathbf{Q}}\; d\hat{\boldsymbol{\xi}}\,, \tag{34}$$

in which, upon the introduction of the notations $\xi = \xi_1$, $\xi_2 = \eta$ and $\xi_3 = \tau$, the matrix $\hat{\mathbf{Q}}$ can be expressed as (compare with Equation (27)),

$$\hat{\mathbf{Q}} = (Q_{ij}) = \left(\frac{\partial \xi_j}{\partial q_i}\right), \quad i,j = 1,2,3. \tag{35}$$

We now observe that, by the very definition of the ray-centered coordinates along the central (image) ray computed at D, we have

$$Q_{13} = Q_{23} = Q_{31} = Q_{32} = 0 \quad \text{and} \quad Q_{33} = v = v(q_1, q_2, q_3)\,. \tag{36}$$

Substitution into Equation (35) produces the simpler expression of $\hat{\mathbf{Q}}$

$$\hat{\mathbf{Q}} = \begin{bmatrix} & \mathbf{Q} & 0 \\ & & 0 \\ 0 & 0 & v \end{bmatrix}, \tag{37}$$

in which $\mathbf{Q}$, represents the upper left 2×2 submatrix of the matrix $\hat{\mathbf{Q}}$

$$\mathbf{Q} = \begin{bmatrix} Q_{11} & Q_{12} \\ Q_{21} & Q_{22} \end{bmatrix}. \tag{38}$$

In addition, by the elementary rules of matrix calculus, the inverse matrix $\hat{\mathbf{Q}}^{-1}$ is readily found to be

$$\hat{\mathbf{Q}}^{-1} = \begin{bmatrix} & \mathbf{Q}^{-1} & 0 \\ & & 0 \\ 0 & 0 & 1/v \end{bmatrix}, \tag{39}$$

with the understanding that $\det \mathbf{Q} \neq 0$.

Determination of the gradients: We are now ready to determine the gradient components of the sought-for matrix $\hat{\mathbf{\Lambda}}$ in Equation (25). For that, we use Equations (34) and (39), namely

$$d\hat{\boldsymbol{\xi}} = \hat{\mathbf{Q}}^{-1} d\hat{q} = \begin{bmatrix} & \mathbf{Q}^{-1} & 0 \\ & & 0 \\ 0 & 0 & 1/v \end{bmatrix} d\hat{q}\,. \tag{40}$$

If we now introduce the matrix $\hat{\mathbf{V}} = (V_{ij})$, defined by

$$\hat{\mathbf{V}} = \hat{\mathbf{Q}}^{-T}\hat{\mathbf{Q}}^{-1}\,, \tag{41}$$

we find, using Equations (29), that

$$V_{ij} = (\nabla_q \xi_i) \cdot (\nabla_q \xi_j)\,. \tag{42}$$

In view of Equations (33) and (25), it follows that

$$V_{ij} = (\nabla_q \xi_i) \cdot (\nabla_q \xi_j) = (\nabla_x \xi_i) \cdot (\nabla_x \xi_j) = \mathbf{\Lambda}_{ij}\,. \tag{43}$$

As a consequence, we have

$$\hat{\mathbf{V}} = \hat{\mathbf{Q}}^{-T}\hat{\mathbf{Q}}^{-1} = \hat{\mathbf{\Lambda}}\,, \tag{44}$$

from which

$$\hat{\mathbf{\Lambda}} = \begin{bmatrix} \mathbf{Q}^{-1} & 0 \\ 0 \quad 0 & 1/v \end{bmatrix}^T \begin{bmatrix} \mathbf{Q}^{-1} & 0 \\ 0 \quad 0 & 1/v \end{bmatrix} = \begin{bmatrix} (\mathbf{Q}^T\mathbf{Q})^{-1} & 0 \\ 0 \quad 0 & 1/v^2 \end{bmatrix}. \tag{45}$$

Substituting into Equation (24), we obtain the modeling eikonal equation

$$(\hat{\nabla}_\xi Z)^T \begin{bmatrix} (\mathbf{Q}^T\mathbf{Q})^{-1} & 0 \\ 0 \quad 0 & 1/v^2 \end{bmatrix} (\hat{\nabla}_\xi Z) = 1\,. \tag{46}$$

Migration and interval (Dix) time velocities: The velocity, $v = v(\xi, \eta, \tau)$, in the eikonal Equation (46), represents the depth velocity at the point P of the image ray, which is determined by the coordinates (ξ, η, τ) in the time-migration domain. We recall that, in this domain, (ξ, η), specifies the trace and τ the (two-way) time migration sample. As such, the velocity $v(\xi, \eta, \tau)$ is unknown. However, that velocity is related with *interval (Dix) time-velocity matrix*, $\mathbf{V}_{Dix}$, computed from the *time-migration velocity matrix*, $\mathbf{V}_M$, the latter being directly estimated in the prestack time migration process. More specifically, we have the important relation(see Cameron et al., 2007; Gelius and Tygel, 2015),

$$\mathbf{V}_{Dix}^2 = \frac{\partial}{\partial \tau}\left(\frac{\tau}{2}\mathbf{V}_M^2\right) = v^2(\mathbf{Q}\mathbf{Q}^T)^{-1}\,. \tag{47}$$

Computing determinants from both sides of the above equation, and using simple properties of the determinant, it follows that

$$\det \mathbf{V}_{Dix}^2 = (\det \mathbf{V}_{Dix})^2 = v^4(\det \mathbf{Q})^{-2}\,, \tag{48}$$

leading to

$$v^2 = v_{Dix}^2 |\det \mathbf{Q}|, \quad \text{com} \quad v_{Dix}^2 = |\det \mathbf{V}_{Dix}|\,. \tag{49}$$

Substitution into the eikonal (46), and after simple manipulations, we find that

$$(\hat{\nabla}_\xi Z)^T \begin{bmatrix} (\mathbf{Q}^T\mathbf{Q})^{-1} & 0 \\ 0 \quad 0 & \left(v_{Dix}^2 |\det \mathbf{Q}|\right)^{-1} \end{bmatrix} (\hat{\nabla}_\xi Z) = 1\,. \tag{50}$$

It is also useful to write the above equation in non-matrix form. As a first step in that direction, we we readily observe that Equation (50) can be recast as

$$\begin{bmatrix} Z_\xi & Z_\eta \end{bmatrix} (\mathbf{Q}^T\mathbf{Q})^{-1} \begin{bmatrix} Z_\xi \\ Z_\eta \end{bmatrix} + \frac{1}{v_{Dix}^2 |\det \mathbf{Q}|} Z_\tau^2 = 1\,. \tag{51}$$

From the expression of matrix $\mathbf{Q}$ in Equation (38), we write

$$\mathbf{Q}^{-1} = \frac{1}{\det \mathbf{Q}} \begin{bmatrix} Q_{22} & -Q_{12} \\ -Q_{21} & Q_{11} \end{bmatrix}, \tag{52}$$

which, in turn, yields

$$(\mathbf{Q}^T\mathbf{Q})^{-1} = \mathbf{Q}^{-1}(\mathbf{Q}^{-1})^T = \frac{1}{(\det \mathbf{Q})^2} \begin{bmatrix} a & b \\ b & c \end{bmatrix}, \tag{53}$$

with the notations

$$a = Q_{22}^2 + Q_{12}^2, \quad b = -(Q_{11}Q_{12} + Q_{22}Q_{21}), \quad c = Q_{11}^2 + Q_{21}^2 \,. \tag{54}$$

Substitution into the Equation (51), we obtain the the eikonal in non-matrix form

$$a\, Z_\xi^2 + 2b\, Z_\xi Z_\eta + c\, Z_\eta^2 + \frac{|\det \mathbf{Q}|}{v_{Dix}^2} Z_\tau^2 = (\det \mathbf{Q})^2 \,. \tag{55}$$

2D situation: In this situation, the eikonal equation involves only the quantities Z_ξ e Z_τ. In addition, the matrices $\mathbf{Q}$, $\mathbf{V}_M$ e $\mathbf{V}_{Dix}$, reduce to scalars, Q, $V_M = v_M$ e $V_{Dix} = v_{Dix}$. As a consequence, the Equation (47) simplifies to

$$v_{Dix}^2 = \frac{\partial}{\partial \tau}\left(\frac{\tau}{2} v_M^2\right) = v^2 \left(\frac{1}{Q^2}\right) \,. \tag{56}$$

In the same way, the 3×3 matrix, $\hat{\mathbf{\Lambda}}$, reduces to the 2×2, $\mathbf{\Lambda}$ given by

$$\mathbf{\Lambda} = \begin{bmatrix} 1/Q^2 & 0 \\ 0 & 1/(Q^2 v_{Dix}^2) \end{bmatrix} = \frac{1}{Q^2} \begin{bmatrix} 1 & 0 \\ 0 & 1/v_{Dix}^2 \end{bmatrix} \,. \tag{57}$$

That leads to the eikonal

$$\begin{bmatrix} Z_\xi & Z_\tau \end{bmatrix} \begin{bmatrix} 1 & 0 \\ 0 & 1/v_{Dix}^2 \end{bmatrix} \begin{bmatrix} Z_\xi \\ Z_\tau \end{bmatrix} = Q^2 \,, \tag{58}$$

in matrix form, or, alternatively,

$$Z_\xi^2 + \frac{1}{v_{Dix}^2} Z_\tau^2 = Q^2 \,. \tag{59}$$

in non-matrix form.

Locally laterally homogeneous media: This is the where the velocity is assumed to be laterally constant in the vicinity of each image ray. In the 3D situation this implies that

$$\mathbf{Q} = \mathbf{I}, \quad \mathbf{V}_M = v_M \mathbf{I}, \quad \text{and} \quad \mathbf{V}_{Dix} = v_{Dix} \mathbf{I}, \tag{60}$$

where $\mathbf{I}$ is the 2×2 identity matrix and $v_M = v_M(\tau)$ and $v_{Dix} = v_{Dix}(\tau)$ are escalar velocities that depend only on the migration tempo, τ, being independent from the lateral coordinates, (ξ, η). The relation

$$v_{Dix}^2 = \frac{d}{d\tau}\left(\frac{\tau}{2} v_M^2\right) \,, \tag{61}$$

is still valid. Substituting Equation (60) into Equation (49), we have that

$$v^2 = |\det(v_{Dix}\mathbf{I})||\det \mathbf{Q}| = v_{Dix}^2 \,, \tag{62}$$

in which we have used the properties

$$\det(v_{Dix}\mathbf{I}) = v_{Dix}^2 \det \mathbf{I} = v_{Dix}^2, \quad \text{e} \quad \det \mathbf{Q} = \det \mathbf{I} = 1. \tag{63}$$

As a consequence,

$$\det \mathbf{V}_{Dix} = \det(v_{Dix}\mathbf{I}) = v_{Dix}^2 \det \mathbf{I} = v_{Dix}^2 \,. \tag{64}$$

To obtain the eikonal in the present case, we observe that the condition $\mathbf{Q} = \mathbf{I}$ implies that $Q_{11} = Q_{22} = 1$ e $Q_{12} = Q_{21} = 0$, which, in view of Equation (54), yields

$$a = c = 1, \quad \text{e} \quad b = 0 \,. \tag{65}$$

From Equation (55), we have that the 3D eikonal in locally laterally homogeneous media is given by

$$Z_\xi^2 + Z_\eta^2 + \frac{1}{v_{Dix}^2} Z_\tau^2 = 1 \,. \tag{66}$$

The above equation can be used as an approximate solution para the time-to-depth conversion, under the consideration

$$v_{Dix}^2 = |\det \mathbf{V}_{Dix}| = \left| \det \left[\frac{\partial}{\partial \tau} \left(\frac{\tau}{2} \mathbf{V}_M^2 \right) \right] \right| . \tag{67}$$

By means of analogous arguments as before, the corresponding eikonal for the 2D situation is given by

$$Z_\xi^2 + \frac{1}{v_{Dix}^2} Z_\tau^2 = 1 . \tag{68}$$

In that case,

$$v_{Dix}^2 = V_{Dix}^2 = \frac{\partial}{\partial \tau} \left(\frac{\tau}{2} V_M^2 \right) . \tag{69}$$

APPENDIX B: DERIVATION OF MODELING WAVE EQUATION

For a given wave equation, the process for obtaining a corresponding eikonal leads to a unique equation. However, the reciprocal situation is not unique: A given eikonal may correspond to several wave equations. In this situations, it is reasonable to choose the simplest wave equation that corresponds to a give eikonal. In the present case, the simples wave equation associated to the eikonal equation (55) is given by

$$a \frac{\partial^2 \bar{P}}{\partial \xi^2} + 2b \frac{\partial \bar{P}}{\partial \xi \partial \eta} + c \frac{\partial^2 \bar{P}}{\partial \eta^2} + \frac{|\det \mathbf{Q}|}{v_{Dix}^2} \frac{\partial^2 \bar{P}}{\partial \tau^2} - (\det \mathbf{Q})^2 \frac{\partial^2 \bar{P}}{\partial z^2} = 0 , \tag{70}$$

where $\bar{P} = \bar{P}(\xi, \eta, \tau, z)$ represents the "pressure". In the above modeling wave equation, the variable, z, plays the role of the propagation variable. Besides that, $a = a(\xi, \eta, \tau)$, $b = b(\xi, \eta, \tau)$ and $c = c(\xi, \eta, \tau)$, as well as $v_{Dix} = v_{Dix}(\xi, \eta, \tau)$ and $\mathbf{Q} = \mathbf{Q}(\xi, \eta, \tau)$, have the same meaning as before.

We now verify that the above wave equation has ats associated eikonal the Equation (55). To do so, we tentatively consider the z-propagation ray solution

$$\bar{P}(\xi, \eta, \tau, z) = B \; F(z - Z) , \tag{71}$$

where $B = B(\xi, \eta, \tau)$ and $Z = Z(\xi, \eta, \tau)$ represent the amplitude and "traveltime" in z-propagation. Substitution of the above ray solution into the wave equation (17), and after straightforward manipulations, we obtain the expression of the form

$$U_2 \; F''(z - Z) + U_1 \; F'(z - Z) + U_0 \; F(z - Z) = 0 , \tag{72}$$

where $U_2 = U_2(\xi, \eta, \tau)$, $U_1 = U_1(\xi, \eta, \tau)$ and $U_0 = U_0(\xi, \eta, \tau)$ are functional coefficients determined by that substitution. In order that the ray solution (71) effectively satisfies the wave equation (70), we must have that all coefficients U_2, U_1 and U_0 identically vanish. Doe to the fact that we have only two unknowns, $B(\xi, \eta, \tau)$ and $Z(\xi, \eta, \tau)$ (the "pulse", $F(z)$, does not interfere in the problem), we can impose these vanishing conditions to two coefficients only. By the well-accepted assumptions of ray theory, the coefficients to be chosen to zero are the ones associated with the higher-order derivatives of F, namely U_2 and U_1. The reason for that is that these coefficients are attached to the terms of highest frequency with respect to the propagation variable, z.

The condition $U_2 = 0$ gives rise to the eikonal equation for the function Z, which, in turn, determines the ray trajectories in the propagation variable, z. The condition, $U_1 = 0$, gives rise to the so-called transport equation, that determines the amplitude, B, along the previously determined rays. The coefficient, U_0 is left free in the process. The basic assumption of ray theory is that Equation (71) produces a valid approximate solution of the wave equation.

In our situation, we are interested in the eikonal equation only, which derives from the condition $U_2 = 0$. As can be readily verified, we have

$$U_2 = a \; Z_\xi^2 + 2b \; Z_\xi Z_\eta + c \; Z_\eta^2 + \frac{|\det \mathbf{Q}|}{v_{Dix}^2} Z_\tau^2 - (\det \mathbf{Q})^2 = 0 , \tag{73}$$

which represents the expected eikonal of Equation (55).

REFERENCES

Cameron, M. K., B., F. S., and A., S. J. (2007). Seismic velocity estimation from time migration. *Inverse Problems*, 23:1329–1369.

Cameron, M. K., Fomel, S. B., and A., S. J. (2008). Time-to-depth conversion and seismic velocity estimation using time-migration velocity. *Geophysics*, 73(5):VE205–VE210.

Červený, V. (2001). *Seismic ray theory*. Cambridge University Press.

da Silva, E. F. F., Portugal, R., and Vicentini, A. (2009). Model rays for depth-to-time conversion. In *11th International Congress of the Brazilian Geophysical Society & EXPOGEF 2009, Salvador, Bahia, Brazil, 24-28 August 2009*. Society of Exploration Geophysicists and Brazilian Geophysical Society.

Dell, S., Gajewski, D., and Tygel, M. (2014). Image ray tomography. *Geophysical Prospecting*, 62(3):413–426.

Duveneck, E. (2004). 3D tomographic velocity model estimation with kinematic wavefield attributes. *Geophys Prospect*, 52(6):535–545.

Gelius, L. and Tygel, M. (2015). Migration-velocity building in time and depth from 3D (2D) Common-Reflection-Surface (CRS) stacking - theoretical framework. *Studia Geophysica et Geodaetica*, 59(2):253–282.

Hubral, P. (1977). Time migration - some ray theoretical aspects. *Geophys Prospect*, 25(4):738–745.

Iversen, E. and Tygel, M. (2008). Image-ray tracing for joint 3D seismic velocity estimation and time-to-depth conversion. *Geophysics*, 73(3):S99–S114.

Sava, P. and Fomel, S. (2001). 3-D traveltime computation using huygens wavefront tracing. *Geophysics*, 66(3):883–889.

Tygel, M., Ursin, B., Iversen, E., and de Hoop, M. V. (2011). Estimation of geological dip and curvature from time-migrated zero-offset reflections in heterogeneous anisotropic media. *Geophysical Prospecting*, 60(2):201–216.

Tygel, M., Ursin, B., Iversen, E., and de Hoop, M. V. (2012). Estimation of geological dip and reflector curvature from zero-offset seismic reflections in heterogeneous anisotropic media. *Stud Geophys Geod*, 56(2):521–531.

Ursin, B. (1982). Time-to-depth migration using wavefront curvature. *Geophysical Prospecting*, 30(3):261–280.

Vinje, V., Iversen, E., and Gjøstdal, H. (1993). Traveltime and amplitude estimation using wavefront construction. *Geophysics*, 58:1157–1166.